journal

J. Am. Ceram. Soc., 90 [4] 1130–1138 (2007)
DOI: 10.1111/j.1551-2916.2007.01589.x

Resistance to Thermal Shock and to Oxidation of Metal Diborides–SiC Ceramics for Aerospace Application

Frédéric Monteverde†

CNR-ISTEC, Institute of Science and Technology for Ceramics, National Research Council 48018 Faenza, Italy

Luigi Scatteia

CIRA, Italian Aerospace Research Center, 81043 Capua, Italy

Two SiC-containing metal diborides materials, classified in the ultra-high-temperature ceramics (UHTCs) group, were fabricated by hot-pressing. SiC, sinterability apart, promoted resistance to oxidation of the diboride matrices. Both the compositions, oxidized in air at 1450°C for 1200 min, had mass gains lower than 5 mg/cm^2. Slight deviations from parabolic oxidation kinetics were seen. The resistance to thermal shock (TSR) was studied through the method of the retained flexure strength after water quenching (20°C of bath temperature). Experimental data showed that the (ZrB_2+HfB_2)–SiC and the ZrB_2–SiC materials retained more than 70% of their initial mean flexure strength for thermal quenchs not exceeding 475° and 385°C, respectively. Certain key TSR properties (i.e., fracture strength and toughness, elastic modulus, and thermal expansion coefficient) are very similar for the two compositions. The observed superior critical thermal shock of the (ZrB_2+HfB_2)–SiC composite was explained in terms of more favorable heat transfer parameters conditions that induce less severe thermal gradients across the specimens of small dimensions (i.e., bars 25 mm × 2.5 mm × 2 mm) during the quench down in water. The experimental TSRs are expected to approach the calculated *R* values (196° and 218°C for ZrB_2+HfB_2–SiC and ZrB_2–SiC, respectively) as the specimen size increases.

I. Introduction

TRANSITION metal diborides (MB_2) such as ZrB_2 and HfB_2, commonly referred to as ultra high-temperature ceramics (UHTCs), possess melting temperatures greater than 3200°C. This physical characteristic enables interesting perspectives for applications at temperatures above 1800°C, a typical temperature limit of most structural ceramics. Fields within which ZrB_2 has already found utilizations include induction-heating parts, small crucibles for molten metals, dies for wire-drawing, guides for cold and hot-rolling of alloys and special metal sheets, and high-temperature electrodes. Aerospace research in the past decade has been focused on UHTCs as candidate materials to increase the heat resistance of structural thermal protection systems (TPS) such as leading edges and nose-cones for a new generation of sharp-shaped hypersonic re-entry vehicles.[1–3] Indeed, UHTCs could potentially allow space vehicles to withstand during atmospheric re-entry temperatures in excess of 1800°C, that is widely accepted as the single-use temperature limit of current hot structures materials such as SiC-coated C–C composites.[4] On-ground arc-jet testing has recently shown that UHTCs can be considered an effective enabling technology for sharp-body space vehicles.[2,5,6] Among the family of materials classified as UHTCs, ZrB_2 has a comparatively low density (i.e., 6.09 g/cm^3), and has been addressed as one of the most promising candidates for this specific aerospace application.

The manufacturing of dense MB_2 compacts has typically required the help of applied pressures and prolonged holds in atmosphere-controlled furnaces at sintering temperatures above 2000°C because they own strong covalent bondings and low self-diffusion coefficients.[7,8] Instead, a number of studies has shown that the addition of SiC to MB_2 powders has beneficial effects not only on sinterability,[9–11] but also on mechanical properties[9–12] and resistance to oxidation.[1–3,6,13–16] When MB_2 is exposed to air at elevated temperatures for instance, MO_2 and B_2O_3 are formed, while the volatilization of B_2O_3 above 1200°C leads to the formation of a MO_2 scale.[17–20] SiC containing MB_2-based composites exhibit improved resistance to oxidation compared with the monolithic diboride compacts, thanks to the formation of a silica-based glassy product which covers the faces exposed to air and provides an effective barrier to oxygen transport.

As far as the the resistance to thermal shock (TSR) is concerned, despite the significance of this physical property for the UHTCs group, a lack of data characterizes this subject. Diborides are referred to possess good TSR when compared with other ceramics because of favorable characteristics like the thermal conductivity (i.e., 50–100 $W/m \cdot K$)[21] and strengths up to 1 GPa.[11] Instead, UHTC compositions in the ZrB_2–SiC system reported values in the range of 250°–350°C[22,23] that signify TSR lower than that of a structural ceramic like Si_3N_4.[24,25] It is widely shared that the thermal shock behavior is influenced by a number of mechanical and thermo-physical characteristics like elastic modulus, strength, fracture toughness, thermal expansion, thermal conductivity, and heat transfer rate (i.e. surface conductance).[26] The conditions for crack initiation and propagation have been extensively studied by Hasselman,[27] while a series of parameters was defined to relate thermo-physical and mechanical properties of the materials to their TSR, i.e the so-called thermal stress fracture resistance parameters. The value of thermal shock at which the scattering of the retained strength data significantly spreads out is typically reported as critical thermal shock ΔT_C. Measurements of retained strengths and elastic moduli at room temperature provide indications over the extent of damage after thermal shock.[25,28–30] In addition, different authors argued that size and geometry of the specimens have a substantial impact on the extent of damage induced during thermal shock, verifying that it varies significantly from material to material.[25,26,30–34] A lack of quantitative agreement between (calculated) TSR parameters and experimental ΔT_C was repeatedly pointed out: the importance over such discrepancies of factors like specimen's size and/or geometry and temperature dependence of the heat transfer rate coefficient was assessed.[25,26,33,34]

P. Becher—contributing editor

Manuscript No. 22061. Received July 27, 2006; approved January 9, 2007.
†Author to whom correspondence should be addressed. e-mail: fmonte@istec.cnr.it

Table I. Characteristics of the Commercial Powders Used (Source: Companies Datasheet)

Formula	Company	Type	Density (g cm^{-3})	Particle size	Oxygen (wt%)
ZrB_2	H.C. Starck (Goslar, Germany)	B	6.09	<2 μm	2
HfB_2	Cerac Inc. (Bad Soden-Salmünster, Germany)	325 mesh	11.18	1.7 μm[†]	—
SiC	H.C. Starck	BF 12	3.19	11.6 m^2/g[‡]	0.9
$MoSi_2$	Aldrich (Milwaukee, WI)		6.26	2.8 μm[§]	1

[†]Fisher size (APS). [‡]Specific surface area. [§]Mean value.

The purpose of this study was to measure and compare the TSR of two SiC-containing MB_2-based ceramics, specifically designed as possible base materials for structural aerospace TPSs. In addition, in-air oxidation tests were also performed. Even though similar heat treatments do not fully reproduce the real operative re-entry conditions, the results provided precious complementary informations for the understanding of the oxidation behavior. The materials herein examined were already characterized in their radiative and surface catalytic behavior[35]: thanks to low catalycity and high emissivity, they showed a good potential for the selected application.

II. Experimental Procedure

(1) Materials Processing

Two MB_2–SiC mixtures of commercial powders, amounts in vol%,

$$ZrB_2 + 15SiC \text{ (composition ZSM)}$$
$$ZrB_2 + 15SiC + 10HfB_2 \text{ (composition ZHSM)}$$

were ball-milled in absolute ethyl alcohol for 24 h, using high-purity zirconia milling media. A quantity $<5\%$ of $MoSi_2$ serving as sintering aid was batched into both the compositions. Table I shows some characteristics of the raw powders used. After drying in a rotating evaporator, the powder mixtures were sieved through a mesh screen with 250 μm openings.

The powder mixtures were uniaxially hot-pressed in vacuum using an inductively heated graphite die, lined with a BN-sprayed graphitized sheet. Peak temperatures/dwell times/applied pressures were 1820°C/15 min/30 MPa for ZSM, and 1900°–1940°C/45 min/40 MPa for ZHSM, about 20°C/min average heating rate. The temperature was measured by means of an optical pyrometer focused on the graphite die.

(2) Materials Characterization

(A) Microstructure: The bulk density (d_B) and the theoretical density (d_{TH}) were evaluated using the Archimedes method (water as immersing medium) and the rule-of-mixture, respectively. The relative density (RD) was calculated dividing the bulk density by the theoretical density . The phase composition was analyzed with an X-ray diffractometer (XRD, Ni-filtered Cu$K\alpha$ radiation, model D500, Siemens, Karlsruhe, Germany) and a scanning electron microscope (SEM, model S360, Leica Cambridge, Cambridge, UK) combined with an energy-dispersive X-ray microanalyser (EDX, model INCA Energy 300, Oxford Instruments, Abington, UK). Polished sections of the as-sintered materials were prepared with successively finer diamond-based abrasives ranging from 50 to 0.25 μm. A qualitative estimate of the grain size was made off from SEM images of fracture surfaces.

(B) Properties

(a) Mechanical: The Young's modulus (E) and Poisson's ratio (ν) were measured on a 28 mm × 8mm × 0.8 mm plate using the resonance frequency method. Micro-hardness (HV1.0) was evaluated by a Vickers indenter, using a 9.81 N applied load for 15 s. Flexure strength (σ) in a 4-pt. configuration was tested (model Z050, Zwick/Roell—Ulm, Germany) at room temperature (five specimens) on 25 mm × 2.5 mm × 2 mm chamfered bars using 20 mm and 10 mm as outer and inner span, respectively, and a cross-head speed of 0.5 mm/min. The surface finish of the bars, measured using a contact stylus type profiler (model Talysurf Plus, Rank Taylor Hobson, Leicester, U.K.), was $R_a = 0.14 \pm 0.01$ μm, R_a being the arithmetic mean deviation of the assessed profiles. Fracture toughness (K_{Ic}) was measured through the chevron notched beam method at room temperature (three specimens) using 25 mm × 2 mm × 2.5 mm bars on the same jig used for the flexure strength (cross-head speed 0.02 mm/min). The bars were notched with an 0.08-mm diamond saw; the chevron notch tip depth and the average side length were about 0.12 and 0.8 times the bar thickness, respectively. The "slice model" equation of Munz *et al.* [36] was used for the calculation of K_{Ic}.

(b) Thermo-Physical: Thermal expansion up to 1300°C was evaluated using a dilatometer (model DIL 402E, Netzsch Gerätebau GmbH, Selb, Germany) in a stream of argon, 5°C/min heating rate. Thermal diffusivity (D_{TH}) up to 1200°C was measured through the laser flash method (model LFA-427, Netzsch Gerätebau GmbH), and following the standard EN 821-2 as guideline. Heat capacity (C_P) was measured using a modulated differential scanning calorimetry (model MDSC, TA Instruments, New Castle, DE).

The TSR was studied through the method of the retained flexure strength after water-quenching (20°C of bath temperature and 50°C of thermal quench step). Chamfered bars 25 mm × 2.5 mm × 2 mm were used for testing. The experimental critical thermal shock ΔT_C was determined using the guidelines outlined by the standard prEN820-3. In particular, ΔT_C was identified using a linear interpolation between points that first reduce the average flexure strength of the quenched bars by more than 30% of the mean strength of the as-sintered material. For each quench temperature, at least three specimens were tested. In addition, the variation of the elastic modulus (E_M) on the thermal shocked specimens was estimated using the load-deflection method, and following the standard prEN 843-2 as guideline. A cross-head displacement (recorded during the loading cycle) from 50% of the peak load to 90% of the peak load was selected in order to minimize strong non-linearities.

(c) Resistance to Oxidation: The resistance to oxidation was tested in flowing dry air (20 cm^3/min) at 1450°C for 1200 min, 30°C/min of heating rate and free cooling, using a thermogravimetric analyser (model STA449 Jupiter, Netzsch Gerätebau GmbH, 10^{-3} mg of accuracy) equipped with a vertically heated Al_2O_3 chamber. Spacers of zirconia were placed between the specimens (dimensions 14 mm × 2.5 mm × 2 mm) and the Al_2O_3 holder with minimal contact area. The specimen's mass was measured before and after exposure. XRD and SEM techniques were used to analyze the microstructures of the oxidized samples.

III. Results

(1) Microstructure Development

Table II shows processing parameters and some microstructure features of the hot-pressed materials. The bulk densities d_B of the as-sintered ZSM and ZHSM compacts were 5.61 and 6.06 g/cm^{-3}, respectively. These values of density correspond to relative densities of 99% ZSM and 98.2% ZHSM. The fracture surfaces observed by SEM displayed the grain structure of both the composites, with regularly faceted diboride grains (maximum size 5 μm). Representative regions of fracture sur-

Table II. Processing Parameters and Microstructure Features of the Hot-Pressed Materials: Peak Temperature (T), Dwell Time (t), Maximum Applied Pressure (P), Theoretical (d_{TH}) and Bulk Density (d_B), Relative Density (RD), and Grain Size (GS)

	Processing parameters			Microstructure features			
				Density			
Sample	T (°C)	t (min)	P (MPa)	d_{TH} (g/cm^3)	d_B (g/cm^3)	RD (%)	GS (μm)
ZSM	1820	15	30	5.67	5.61	99.0	2
ZHSM	1940	45	40	6.17	6.06	98.2	3

faces revealed also a high percentage of transgranular versus intergranular fracture between the diboride grains in both the compositions. The XRD analysis of the ZSM compact identified the main phases ZrB_2 and SiC, and an amount of monoclinic zirconia <1 vol%. Instead, in the ZHSM compact, obvious changes in the starting composition took place during sintering. XRD analyses showed the formation of ZrB_2/HfB_2 solid solutions, hereafter indicated as $(Zr,Hf)B_2$. Such solid solutions uphold the hexagonal structure of the initial ZrB_2, but host at the same time Hf atoms. The presence of $(Zr,Hf)B_2$ solid solutions, which very often appear as shells around ZrB_2 cores, is exactly confirmed by the typical configuration of the diboride grains structured in core-shell (Fig. 1). The formation of such $(Zr,Hf)B_2$ s.s. was further assessed through localized EDX analyses on polished surfaces. Furthermore, the polished section examined by SEM highlighted the SiC particulates distributed intergranularly within the diboride matrices, in ZSM sometimes in agglomerates (maximum size 5 μm). At the same time, SEM observations do not provide evidence of residual porosity.

Compared with the ZSM composition, the addition of HfB_2 into the ZHSM composition enhanced refractoriness of the initial powder mixture. In fact, higher peak temperature and longer hold were necessarily applied so far to complete densification: during the hold of 45 min, temperature drifted from 1900° to 1940°C. Such conditions led the grain structure of the ZHSM composition to increase in the average size more than that of the ZSM composition (Table II). Moreover, in ZHSM a partial sintering of the intergranular SiC agglomerates took place. Processing, densification behavior, and microstructure development of similar systems are described in several earlier papers.[9–11,21,24,37]

(2) Mechanical and Thermo-Physical Properties

Tables III and IV and Figs. 2–4 show the experimental data for selected properties. Average values of flexure strength at room temperature (σ_{R0}) of 795 and 765 MPa for the as-sintered ZSM and ZHSM materials, respectively, result better than for a similar system composed of ZrB_2 mixed with 15 vol% SiC and then hot-pressed.[37] The co-existence of very hard components like MB_2 and SiC, along with the fine and dense structure, favored high levels of micro-hardness. However, 4.1 MPa · m$^{1/2}$ as mean value of fracture toughness in both the materials is typical for this family of (brittle) ceramics.[2,9–12,24,37]

The behavior of the retained strength (σ_R) after water-quench is shown in Fig. 2. The σ_R data of the thermal quenched bars in Fig. 2 indicate that a thermal shock severity ΔT_C as high as 385° and 475°C were sustained by ZSM and ZHSM, respectively, before losing more than 30% of their initial mean flexure strength σ_{R0} (Table III). Just for comparison, a ZrB_2 material containing 15 vol% SiC (95% relative density and 235 MPa mean flexure strength), tested using the water-quenching method, reported a TSR of 350°C.[23] It should also be noted that the ZSM specimens quenched above ΔT_C have an evident scatter of strength values above and below the reference threshold (i.e., 70% of the initial mean strength). On the contrary, the ZHSM material seems to follow Hasselman's theory,[27] which predicts a sharp drop in strength at a critical thermal shock temperature difference. The plots in Fig. 3 show the elastic modulus (E_M) of a thermal shocked specimen against its σ_R. A substantial decrease in strength was very often accompanied with a significant reduction in elastic modulus.

In order to confirm that the decrease in flexure strength after quenching was actually an effect of the thermal shock, four specimens of ZSM were heated up to 500°C (5°C/min heating rate), held at that temperature for 15 min to establish thermal equilibrium, and then left cooling freely inside the furnace instead of quenching them into the water bath at 20°C. The retained flexure strength, 850±15 MPa mean±1 standard deviation, measured at room temperature on the heated (and not-quenched) ZSM specimens, did not show significative differences, if compared with σ_{R0} of the pristine material (Table III). This suggests that the decay in flexural strength measured after quenching is primarily caused by thermal shock-induced effects.

The conditions for failure in the pristine material during a thermal quench is usually predicted by setting the maximum permitted thermally-induced stress equal to its tensile or bend strength. Table IV lists two TSR parameters calculated from Eqs. (1) and (2)

$$R = \sigma(1-\nu)/(\alpha E) \quad (1)$$

$$R' = RK_{TH} \quad (2)$$

where σ, ν, α, E, and K_{TH} represent modulus of rupture, Poisson's ratio, coefficient of thermal expansion, elastic modulus, and thermal conductivity, respectively. The comparison of the TSR values in Table IV shows that the calculated R values are much lower than the experimental ΔT_C.

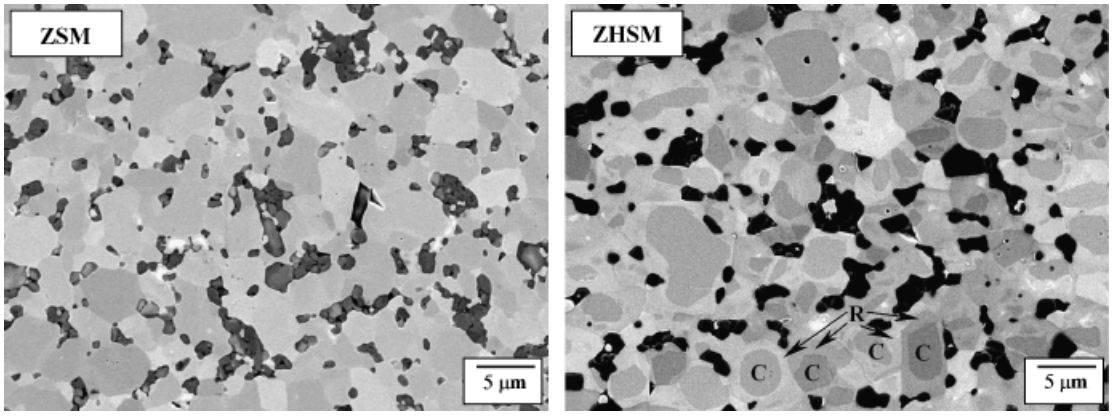

Fig. 1. Polished cross-sections of ZSM and ZHSM (SEM micrographs, secondary electrons); dark features are SiC particles. The core (C)– rim (R) structure in ZHSM is indicated.

Table III. Mechanical Properties of the Hot-Pressed ZSM and ZHSM Materials: Elastic Moduli E (Resonance Frequency Method) and E_{M0} (Load-Deflection Method), $\Delta E = (E–E_{M0})/E$, Poisson's Ratio ν, Micro-Hardness HV1.0, Fracture Toughness K_{Ic}, and Flexure Strength at Room Temperature σ_{R0}

Sample	$E^{\dagger}$ (GPa)	$E_{M0}{}^{\ddagger}$ (GPa)	ΔE (%)	ν	‡HV1.0 (GPa)	‡K_{Ic} (MPa$\sqrt{}$m)	‡σ_{R0} (MPa)
ZSM	480±4	444±5	7.5	0.12	17.7±0.4	4.1±0.05	795±105
ZHSM	508±4	473±9	6.9	0.128	18.2±0.5	4.1±0.75	765±75

†Uncertainity. ‡Mean±1 standard deviation.

Table IV. Thermo-Physical Properties and TSR Parameters (R and R') of the Hot-Pressed ZSM and ZHSM Materials: Linear Coefficient of Thermal Expansion α (25°–1300°C), Thermal Conductivity K_{TH}, and Critical Thermal Shock ΔT_C

		K_{TH}(W/m·°C)				TSR parameters			
							†R' (kW/m)		
Sample	α (10^{-6}/°C)	30°C	500°C	1000°C	1200°C	†R (°C)	30°C	500°C	ΔT_C (°C)
ZSM	6.68	62.5	64.5	65.1	65.2	218	13.6	14.0	385
ZHSM	6.74	79.9	83.5	84.2	85.0	196	15.7	16.4	475

†Calculated using σ_{R0} in Eq. (1). TSR, resistance to thermal shock.

Discrepancies between calculated R values and observed ΔT_C have been reported previously by many investigators,[25,26,33,34] and may indicate that cracks initiate under the so-called soft thermal shock. These conditions imply that the interior of the specimens cools before the surface, resulting in the need for a stress reduction factor determined using the so-called Biot modulus $\beta = Lh/K_{TH}$ (L characteristic specimen's length, K_{TH} thermal conductivity, and h surface heat transfer coefficient between specimen and cooling medium). The R parameter captures the initiation of thermal shock cracking under hard thermal shock conditions (i.e., values of $\beta > 20$[26]): higher values of R are in favor of greater resistance to fracture initiation during quenching. Differences between R and ΔT_C are particularly evident for water-quenching thermal shock tests, primarily because of the dramatic reduction in heat transfer coefficient after the formation of protective steam bubbles at the water/specimen interface: such a phenomenon would mitigate the severity of thermal shock, and result in overestimated ΔT_C values, compared to the expected R parameter.[33]

The thermal conductivity (K_{TH}) was calculated using the expression $K_{TH} = D_{TH}C_P\rho$, where D_{TH}, C_P, and ρ represent thermal diffusivity (Fig. 4), heat capacity (Fig. 4), and density, respectively. Within the interval 30°–1200°C, the calculated data indicate that ZHSM tends to dissipate heat faster than ZSM (Table IV). Just for comparison, such values of K_{TH} result lower than that reported for a ZrB_2+20%SiC, i.e., 103.8 W/m°C at RT.[38] In the present case of small sized specimens and significant K_{TH} (i.e., low values of β), the TSR ranking is more adequately determined by the R' parameter (Table IV). It is, however, expected that in increasing L (i.e., the minimum heat transfer (specimen) dimension or its thickness in the case of standard flexure bar) the observed ΔT_C values begin to approach the correspondent R parameters (see Table IV), minimizing the differences between the two tested compositions.

(3) Resistance to Oxidation

The graphical trends of the specific mass change (w) versus time (t) during the 1200 min exposure at 1450°C is plotted in Fig. 5, 3.43±0.02 and 4.88±0.02 mg/cm^2 being the final w values for ZSM and ZHSM, respectively. Offsets equal to 0.47±0.02 and 0.4±0.02 mg/cm^2, which account for some oxidation prior the 1200 min hold, were respectively subtracted from raw data of ZSM and ZHSM. Some data processing was done by calculating the dummy constant $K_D = w^2/t$ (Fig. 6). Such an exercise points out that during the isothermal exposure obvious parabolic kinetics (i.e., slope of the log K_D equal to zero) were never established. In addition, the analysis of the very early stages of the isothermal hold (see inset in Fig. 5) shows however prevailing mass loss mechanisms over mass gain mechanisms, which in turn become typical for the remaining exposure.

The XRD analyses on the surfaces exposed to air revealed monoclinic MO_2, M = Zr for ZSM, and Zr/Hf for ZHSM, while the cross-sections emphasized a structure that consists of an outermost glassy layer on top of a sub-scale composed of MO_2 crystals (partially embedded within the same glass), which extends up to the unoxidized bulk (Fig. 7). The glassy layer, whose composition analysed by SEM–EDX falls in the Si–O system, adheres to the sub-scale, even though its thickness varies from few to some tenths of microns. The values of about 50 and 100 μm are grossly representative of the oxide sub-scale thickness for ZSM and ZHSM, respectively. In addition, EDX analyses assessed that, in proximity of the interface between oxide sub-scale and unoxidized bulk (Fig. 8), sites formerly occupied by SiC particulates now appear occupied by a carbon-based solid compound. Such an oxidation by-product, whose occurrence was already reported,[10] was connected to the active oxidation of SiC, which induces a partial depletion of SiC close to the inner oxidation front facing the virgin bulk. Such an oxidation mechanism creates so far porosity within the sub-scale formerly mentioned.

IV. Discussion

(1) Microstucture and TSR

Contrary to the well-known limitations connected to the densification of MB_2-based materials,[5,8–11,39] the obtainment of near full dense compacts was allowed by SiC which substantially enhanced densification of MB_2 during hot-pressing. Similarly to powders of TiB_2,[40,41] MO_2 and B_2O_3 were assumed as the main oxygen carriers upon the surfaces of MB_2, M = Zr and Hf. Such a contamination by oxygen promotes vapor phase transport (and thus coarsening) at temperatures below which mass transfer mechanisms like boundary/volume diffusion, which are much more effective than vapor phase for densification, start taking place: the anticipated coarsening decreases the driving force for densification at higher temperatures. Densification of SiC-containing MB_2 powder mixtures initiates at lower temperatures compared with pure MB_2[10,42] as reactions with SiC are deemed to remove the oxide coatings separating MB_2 particles from mutual contact.

As far as the TSR evaluated through the retained strength after water-quenching is concerned, the superior ΔT_C in the ZHSM material, compared with that of ZSM material, was attributed to more favorable heat transfer parameters conditions

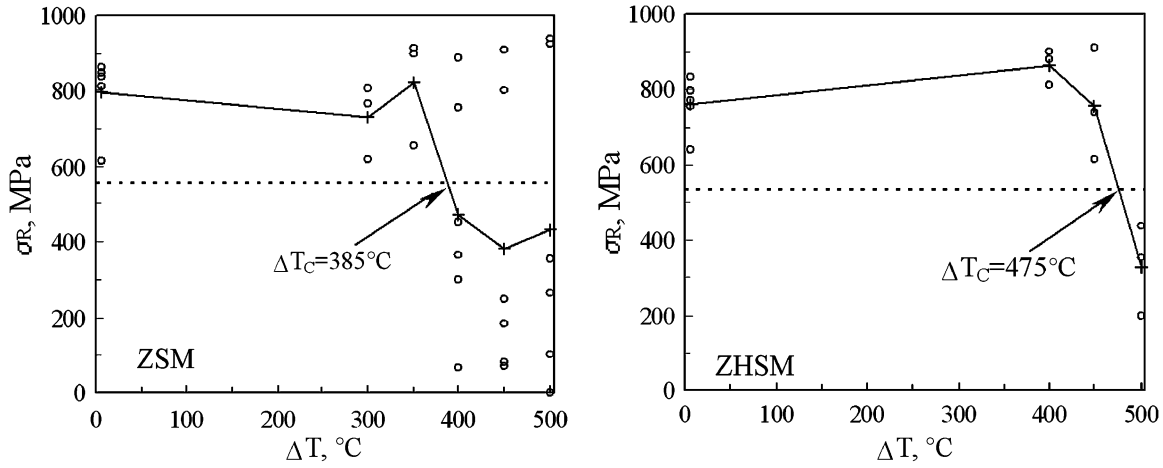

Fig. 2. Retained flexure strength (σ_R) vs. thermal shock (T) of ZSM and ZHSM in water bath at 20°C; full lines connect mean σ_R values at each T tested. Horizontal dashed segments: 70% σ_{R0} of ZSM and ZSM and ZHSM (see Table III).

that induce less severe thermal gradients across the specimen during the quench down test in a 20°C water-bath. Being all the specimens tested of the same (small) dimensions, the different K_{TH} (Table IV) was deemed to modify the actual Biot moduli of the two composites during quenching. It can at first be noticed that large fracture toughness (K_{Ic}) to strength (σ) ratios represent a favorable material's characteristic for minimizing the extent of the crack propagation, but stands in direct contrast with the requirement of high strain-to-failure necessary for preventing crack initiation.[26,27,43] Hence, the combination of large E and σ values which pertains the present materials may induce deleterious damage resulting from fracture if it does occur upon severe thermal shocking, i.e., above ΔT_C. It was in fact observed that, for thermal quench above ΔT_C, a ZSM specimen spalled into a number of pieces, i.e., it had no measurable retained strength. This situation very likely arose because of the sudden release of the large thermal strain-energy required to initiate a crack from very small flaws in the material.

The observed ΔT_C for ZSM and ZHSM, respectively, seem to contradict the expected ranking based on the calculated R parameters. Lewis has stressed the importance of selecting the most appropriate value for strength so that meaningful rankings can be settled.[34] In addition, Becher *et al.* argued that, as does the size dependence of the strength of ceramics, the temperature dependence of thermal conductivity and surface heat transfer coefficient varies with temperature for different materials.[33] Unfortunately, surface heat transfer coefficients usually are not known precisely and have been shown, moreover, to vary over three orders of magnitude within the typical temperature range of water-quench tests. Therefore the actual ΔT_C values for essentially all materials are function of the heat-transfer conditions, and are not solely dependent on materials characteristics. Furthermore, the determination of adequate strength values, such as the Weibull lower limiting strength, is known to require extensive testing. On the other hand, when extensive strength data from appropriately sized specimens are unavoidable (this is the present case), reasonable success can be obtained by taking a characteristic strength as the mean value less two or three standard deviations.[45] Calculated R values and experimental ΔT_C under regimes of soft thermal quenchs have been repeatedly correlated through empirical expressions $\Delta T_C = f(\beta) \cdot R$ which try to approximate the thermal stress solutions for specific sample geometries of rod, plate, or bar.[25,26,30,33,34] Also for the present study, an empirical approach was adopted (damping factor $f(\beta) = 1 + B/\beta$, $0 < 1/f(\beta) < 1$, $\beta = Lh/K_{TH}$, h surface heat transfer coefficient, L minimum specimen dimension, K_{TH} thermal conductivity, and B shape factor). According to the Lewis criterion,[45] the mean strengths σ_{R0} less three standard deviations (named σ_{ZSM} and σ_{ZHSM} in Fig. 9) were used for calculating corrected R parameters for ZSM (R_{ZSM}) and ZHSM (R_{ZHSM}), respectively. By setting $L = 2$ mm, $B = 4$, and $K_{TH} = 83.4$ W/m · K at 475°C for ZHSM, an effective h of 67 kW/m^2 · °C was inferred, being $\beta \cong 1.6$ in correspondence of ΔT_C equal to 475°C. This guess for the h parameter, though merely practical for such a comparison, falls anyhow very close to the typical range of values for ceramics during water-quenching thermal shock tests,[34,44] in particular 50 kW/m^2 · °C for TiB_2 at 500°C of thermal water-quench.[44] Keeping the same values of h and L for ZSM, the reduced K_{TH} value of 64.2 W/m · °C at 385°C (that means β approaching 2.1) induces more severe thermal gradients in the quenched specimens, leading to a less effective capacity to withstand thermal stresses (i.e., ΔT_C approaching 385°C). Being

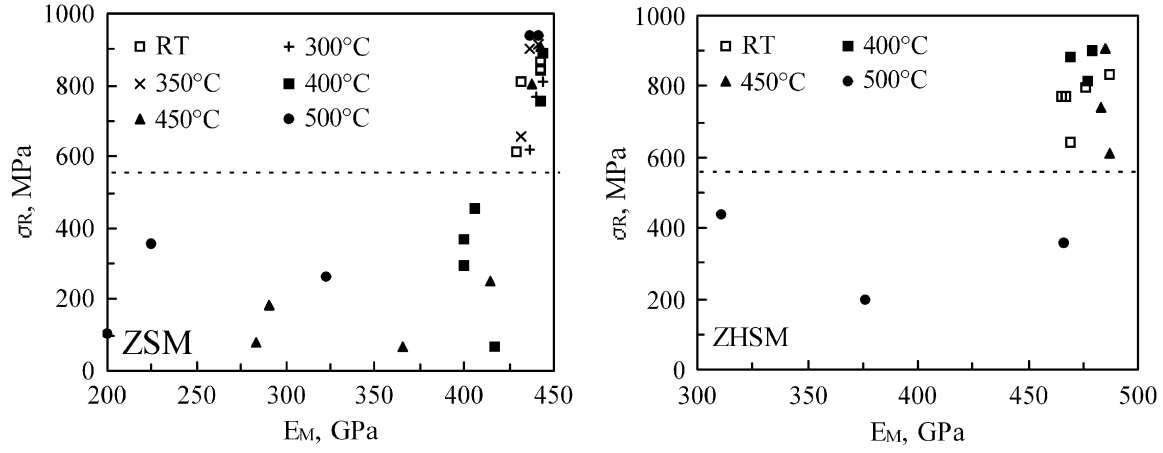

Fig. 3. Retained flexure strength (σ_R) vs. residual elastic modulus (E_M) of bars thermal shocked in water bath at 20°C. Horizontal dashed segments: 70% σ_{R0} of ZSM and ZHSM (see Table III).

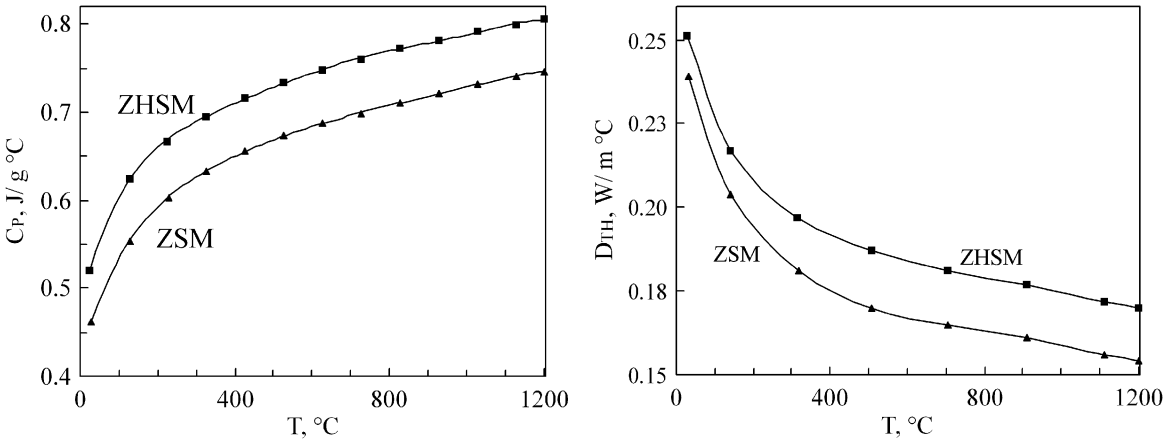

Fig. 4. Heat capacity (C_P) and thermal diffusivity (D_{TH}) vs. temperature (T) of ZSM and ZHSM up to 1200°C.

the dimensions of the specimens nominally identical, such a difference in ΔT_C can thus be connected to the superior thermal conductivity that in the ZHSM material modulates a more favorable damping factor $f(\beta)$ through the Biot number. It is also expected that, having both the composites levelled characteristics like strength, Poisson's ratio, fracture toughness, thermal expansion and elastic modulus, the observed ΔT_C parameters approach the calculated R values of about 200°–220°C in components of larger dimensions.

In Fig. 3, the sharp reduction in elastic modulus E_M was very often accompanied with a significant decrease in the retained strength σ_R. The general agreement between the reduction of flexure strength to coincide with a loss of elastic modulus makes such combined measurements a useful tool to correlate the severity of the damage introduced during a thermal quench with the capacity to withstand further external loads. Experimental data in Fig. 3 clearly show that σ_R results more susceptible than E_M to the influence of newly formed flaws during thermal shock. According to the Griffith relation among strength σ, fracture toughness K_{Ic} and flaw size c, $\sigma \approx K_{Ic}/\sqrt{c}$, the initiation and growth in size of just a single flaw after thermal shock have more obvious effects on strength than on elastic modulus.[46] Evidence of it is in both the compositions, when the elastic modulus declines less or not at all, compared with the corresponding σ_R values which exceeded an absolute loss of more than 30% σ_{R0} (Table III). Therefore, for apparent drops of the elastic modulus, the corresponding strength decay is very likely connected to a substantial damage initiated and grown during thermal shock in form of random network of cracks.

A significantly larger scatter in retained strength differentiates ZSM material from ZHSM material (Fig. 3). Also, the strength scatter is associated to concurrent large scatter in retained elastic moduli: there is no thorough explanation for this. On one hand, to the authors' knowledge, a similar behavior in analogous systems was not verified. In ZSM material, the concomitant occurrence of large scatter in retained values of strength and elastic modulus (Figs. 2 and 3) may be indicative of a non-uniform growth in cracks density and/or size due to sub-critical crack propagation in the water quench bath. On the other hand, the quench experiments have some well-recognized limitations. The TSR tests herein adopted require for instance sample geometries that are amenable to subsequent mechanical testing, and many specimens should be tested to assure the significance of the results. In addition, the specimens are tested destructively: this implies that initiation sites and sub-critical thermal damage are difficult to identify. Thermal stress gradients across the small sized specimens may therefore contribute to the variability of the retained strength after quenching above ΔT_C due to the probability of a initiation site being positioned in the high stress locations. It is known in fact that the flexure strength testing reaches the maximum stress only close to the specimen's surface. The combination of the thermo-mechanical characteristics in the ZHSM material is somewhat more beneficial for a superior TSR as compared with that of the ZSM material, especially for the small specimens herein tested. However, the absence of a large scatter in retained strength and elastic modulus with increased thermal shock seen for the ZSM composite offers a real advantage for the ZHSM material. More extensive testing and characterizations would assist in identifying the difference in damage mechanisms and the benefits of such behavior.

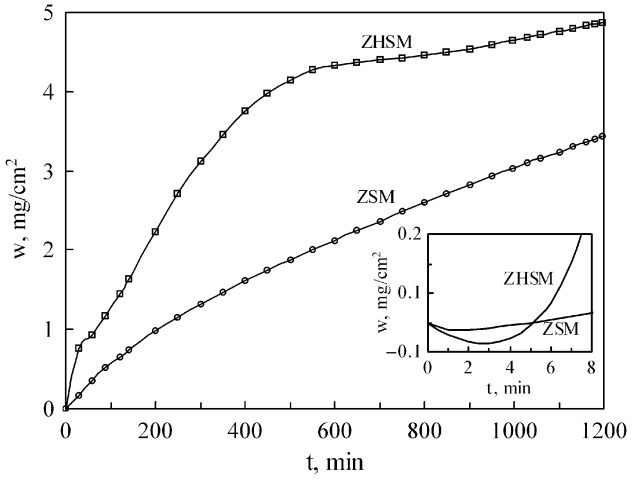

Fig. 5. Specific mass change (w) vs. exposure time (t) during oxidation at 1450°C. The inset expands the very early stages of the isothermal hold.

(2) The Resistance to Oxidation

The negative oxidation rate along the very early stages of exposure at 1450°C (see inset in Fig. 5) discloses that the oxidation of MB_2

$$MB_2 + 5/2\,O_2(g) = MO_2 + B_2O_3(l) \quad (3)$$

is however dominated by the volatilization of boron oxide

$$B_2O_3(l) = B_2O_3(g) \quad (4)$$

from the specimen's surfaces exposed to the air-atmosphere. Reactions 3 and 4 describe mechanisms of weight gain and weight loss, respectively.

With increasing exposure time, the resistances to oxidation of both the composites, due to SiC which is known to start oxidizing more slowly than MB_2, begin taking advantage from the ongoing formation of a glass coating on the faces exposed to air (Fig. 7). Generally SiC, according to the reaction

$$SiC + 3/2\,O_2(g) = SiO_2 + CO(g) \quad (5)$$

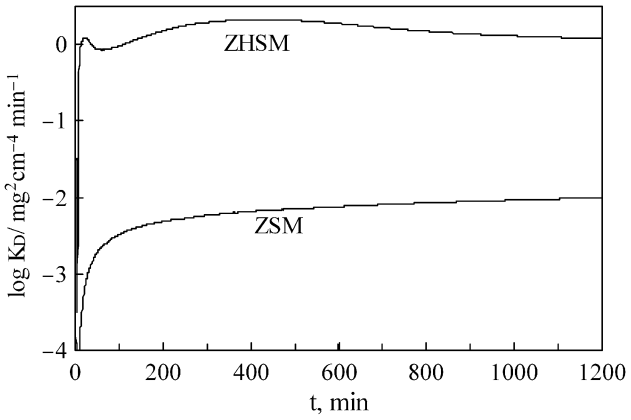

Fig. 6. Dummy parameter K_D vs. exposure time (t), $K_D = w^2/t$.

reacts with oxygen and provides silica. Similarly to other ZrB_2–SiC systems,[1,3,6,10,13,15,16,24,47] significant amounts of silica combine with the available B_2O_3 and yield a borosilicate glass. Such a glassy oxidation product is deemed to lose progressively the B_2O_3 component, but is capable of providing better protection against oxidation than an MO_2-based scale covered with only boron oxide.[6] Although the borosilicate glass behaves as excellent oxidation barrier below 1600°C, it softens, due to the diminished viscosity. The undulating pattern of the external glass is ascribed to the reduced viscosity.

The marked difference of the thermo-gravimetric curves in Fig. 5 is still a matter of reasoning. The evaluation of the specific weight changes could have been underestimated because of phenomena connected to simultaneous gains and losses of mass, which a previous work on the ZrB_2–SiC system firmly asserted.[15] The initial faster mass gain rate in ZHSM was attributed to an inadequate provision of protective glass, compared to ZSM, coupled with an easier diffusion of oxygen along short-circuited paths through the forming $(Zr,Hf)O_2$ sub-scale. Next, the reason why, compared to ZHSM, ZSM better resisted against oxidation remains unclear. Having both the compositions the same nominal content of SiC and negligible levels of porosity, the core-shell structure of $(Zr,Hf)B_2$ solid solutions in ZHSM supposedly was thought to offer less resistance to the inward diffusion of oxygen, compared to ZrB_2.

Even though an oxidation process governed by the oxygen diffusion through a glass that fits parabolic kinetics seemed a logic expectation, departures from an ideal parabolic pattern were instead of not marginal significance (Fig. 6). A number of factors is indicated responsible of such deviations: the evolution of volatile products (B_2O_3, CO), non-steady state behavior due to faster oxidation of MB_2 compared with SiC, and the active

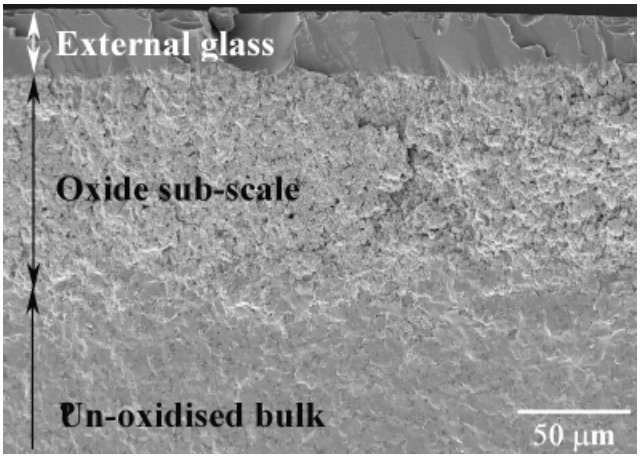

Fig. 7. Fracture cross-section of the ZHSM material after 1200 min at 1450°C in air (SEM micrograph, secondary electrons). An oxide sub-scale (100 m thick) underlying the external glass (25 m thick) is indicated.

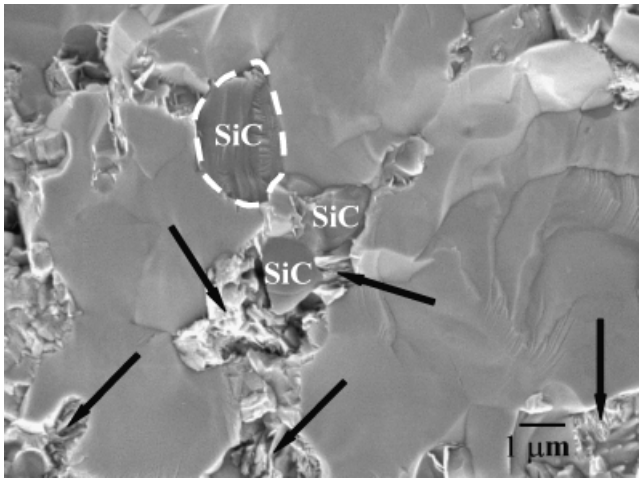

Fig. 8. ZHSM material after 1200 min at 1450°C in air; SEM micrograph, secondary electrons. SiC particles and carbon-based by products (arrows) near the oxide sub-scale/unoxidized bulk interface are shown.

oxidation of SiC. The last factor remains being explained thoroughly. The examination through the SEM–EDX technique of the sub-oxide scale/diboride interface (i.e across the inner oxidation front) revealed inclusions containing carbon (Fig. 8). Being the size, shape, and distribution referable to the SiC particulates in the unoxidized material, these carbon-based structures were associated with an active oxidation mechanism of SiC. Unlike some authors who claimed the complete volatilization of SiC through active oxidation in SiC-containing MB_2 matrices,[6,15,24] the detection of C in such solid inclusions led to consider the following thermodynamic equilibrium

$$SiC + SiO_2 \Leftrightarrow 2SiO(g) + C \tag{6}$$

as the transition mechanism by which SiC starts experiencing the active decomposition.[48] The reason why SiC transforms in agreement with equilibrium 6 is not fully understood. Most recently, Fahrenholtz developed a thermodynamic analysis of the ZrB_2–SiC oxidation[49]: once SiC starts oxidizing according to reaction (7)

$$SiC + O_2 \Leftrightarrow SiO(g) + CO(g) \tag{7}$$

CO may further reduce to solid *C* at the so called sooting limit (see reaction 8)

$$2CO(g) \Leftrightarrow C + O_2(g) \tag{8}$$

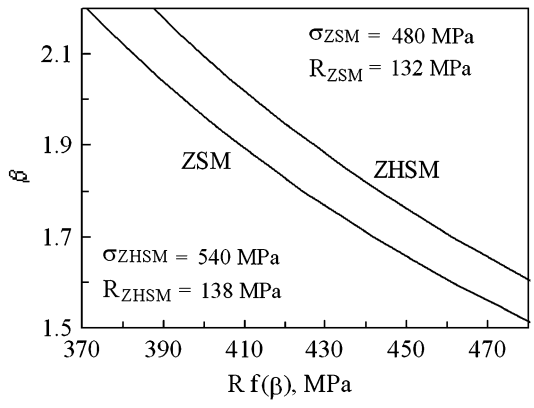

Fig. 9. Biot number β vs. R parameter corrected via damping factor $f(\beta) = 1+4/\beta$. According to Lewis criterion,[45] σ_{ZSM} and σ_{ZHSM}, are σ_{R0} of ZSM and ZHSM, respectively, less 3 standard deviations (see Table III). R_{ZSM} and R_{ZHSM} are obtained by using σ_{ZSM} and σ_{ZHSM} in Eq. (1).

In both cases, it is as much as plausible that conditions of high temperature and low oxygen partial pressure inside the oxidized scale were met for the active oxidation of SiC.[6,49,50] Furthermore, once SiO(g) diffuses outward and encounters a higher oxygen partial pressure, it would further convert into the condensed silica phase. Glass pockets inside the oxide sub-scale but in the vicinity of the external glass may be convincing evidence of the phenomenon just described. It should also be considered that the lack not only of open porosity but also of easily-oxidizable secondary phases is a favorable condition that does not offer preferential paths like pores or grain-boundary channels to the inner transport of oxygen. As a consequence, the oxygen partial pressure P_{O_2} inside the bulk remains at a level sufficiently low to induce the active oxidation of SiC. The P_{O_2} parameter in fact is widely recognized as one of the primary factors controlling the active-to-passive oxidation transition of SiC.[48–51] Such an instability of SiC could have not negligible influence on MB_2–SiC systems in oxidizing conditions, dictating limited durability for prolonged services in thermally harsh applications.

V. Summary

The present work explored the resistance to thermal shock and to oxidation of two ultra-high-temperature MB_2+15 vol% SiC composites, M = Zr and Zr+Hf, brought to full density via hot-pressing. The microstructures were rather uniform (2–3 μm grain size), with SiC incorporated intergranularly within the diboride matrices. The presence of SiC promoted the resistance to oxidation of the diboride matrices through the coverage of a silica-based glass which behaved as an effective barrier against oxidation at high temperature. Both the compositions, oxidized at 1450°C for 1200 min, had specific mass gains lower than 5 mg/cm^2. Deviations from parabolic oxidation kinetics were seen, and attributed to evolution and release of volatile products, to non-steady state behavior based on the faster oxidation of MB_2 compared with SiC, and to active oxidation of SiC. The passive-to-active transition in the oxidation behavior of SiC makes the durability of these SiC-containing diborides-based composites in long-term thermally severe applications an issue. The TSR, tested through the retained strength after water-quench, showed that the ZrB_2–SiC and (ZrB_2+HfB_2)–SiC materials retained more than 70% of their initial mean strength (i.e., ΔT_C) once the thermal shock has not exceeded 385° and 475°C, respectively. On the contrary, the calculated R parameter for the ZrB_2–SiC and (ZrB_2+HfB_2)–SiC materials were 218° and 196°C, respectively. The improved ΔT_C in the (ZrB_2+HfB_2)–SiC was explained in terms of more favorable heat transfer parameters conditions that establish less critical thermal gradients across the specimens of reduced dimensions (i.e., bars 25 mm × 2.5 mm × 2 mm) during a quench down test. Having both the composites key characteristics like strength, fracture toughness, elastic modulus, and thermal expansion very similar, the critical resistance to thermal shock of larger specimens is expected to approach the calculated R parameters.

Acknowledgments

The experimental activities were conducted within the frame of the Unmanned Space Vehicle (USV) Italian National Program. The authors wish to acknowledge the support of C. Melandri (ISTEC, thermal shock tests), A. Balbo (ISTEC, oxidation tests), G. Cosentino (CIRA, heat capacity tests), and M. Tului (CSM, Rome, Italy) for thermal diffusivity tests.

References

[1]K. Upadhya, J.-M. Yang, and W. P. Hoffman, "Materials for Ultra-High Temperature Structural Applications," *Am. Ceram. Soc. Bull.*, **58**, 51–6 (1997).

[2]M. Gasch, D. Ellerby, E. Irby, S. Beckman, M. Gusman, and S. Johnson, "Processing, Properties and Arc-Jet Oxidation of Hafnium Boride/Silicon Carbide Ultra High Temperature Ceramics," *J. Mater. Sci.*, **39**, 5925–37 (2004).

[3]C. Wang, J.-M. Yang, and W. P. Hoffman, "Thermal Stability of Refractory Carbide/Boride Composites," *Mater. Chem. Phys.*, **74**, 272–81 (2002).

[4]H. Pfeiffer and K. Peetz, *All Ceramic Body-Flap Qualified for Space Flight on the X-38, Proceedings of the 53rd International Astronautical Congress*, Houston, 2002.

[5]R. Loehman, "Ultrahigh Temperature Ceramics for Hypersonic Vehicle Applications," *Industrial Heating*, January (2004).

[6]A. Chamberlain, W. Fahrenholtz, G. Hilmas, and D. Ellerby, "Oxidation of ZrB_2–SiC Ceramics Under Atmospheric and Re-Entry Conditions," *Refrac. Appl. Transact.*, **1** [2] 1–8 (2005).

[7]E. Wuchina, M. Opeka, S. Causey, K. Buesking, J. Spain, A. Cull, J. Routbort, and F. Guitierrez-Mora, "Designing for Ultrahigh-Temperature Applications: The Mechanical and Thermal Properties of HfB_2, HfCx, HfN and αHf(N)," *J. Mater. Sci.*, **39**, 5939–49 (2004).

[8]H. Pastor, "Metallic Borides: Preparation of Solid Borides—Sintering Method and Properties of Solid Bodies"; pp. 457–93 in *Boron and Refractory Borides*, Edited by V. I. Matkovich. Springer Verlag, New York, 1977.

[9]F. Monteverde, S. Guicciardi, and A. Bellosi, "Advances in Microstructure and Mechanical Properties of Zirconium Diboride Based Ceramics," *Mater. Sci. Eng.*, **A346**, 310–9 (2003).

[10]F. Monteverde, "Beneficial Effects of an Ultra-Fine α-Sic Incorporation on the Sinterability and Mechanical Properties of ZrB_2," *Appl. Phys. A*, **82**, 329–37 (2006).

[11]A. Chamberlain, W. Fahrenholtz, and G. Hilmas, "High-Strength Zirconium Diboride-Based Ceramics," *J. Am. Ceram Soc.*, **87** [6] 1170–2 (2004).

[12]F. Monteverde and A. Bellosi, "Efficacy of HfN as Sintering Aid in the Manufacture of Ultrahigh Temperature Metal Diborides Matrix Ceramics," *J. Mater. Res.*, **19** [12] 3576–85 (2004).

[13]M. Opeka, I. Talmy, and J. Zaykoski, "Oxidation-Based Materials Selection for 2000°C+Hypersonic Aerosurface: Theorethical considerations and historical experience," *J. Mat. Sci.*, **39**, 5887–904 (2004).

[14]J. Hinze, W. Tripp, and H. Graham, "The High-Temperature Behavior of a Hfb_2+20 v/o Sic Composite," *J. Electrochem. Soc: Solid-State Sci. Technol.*, **122** [9] 1249–54 (1973).

[15]W. Tripp, H. Davis, and H. Graham, "Effect of an SiC Addition on the Oxidation of ZrB_2," *Am. Ceram. Soc. Bull.*, **52** [8] 612–6 (1973).

[16]F. Monteverde and A. Bellosi, "Oxidation of ZrB_2 Based Ceramics in Air," *J. Electrochem. Soc.*, **150** [11] B552–9 (2003).

[17]J. B. Berkowitz-Mattuck, "High-Temperature Oxidation: III. Zirconium and Hafnium Diborides," *J. Electrochem. Soc.*, **113** [9] 908–14 (1966).

[18]A. K. Kuriakose and J. L. Margrave, "The Oxidation Kinetics of Zirconium Diboride and Zirconium Carbide at High Temperatures," *J. Electrochem. Soc.*, **111** [7] 827–31 (1964).

[19]W. Tripp and H. Graham, "The Thermogravimetric Study of the Oxidation of Zrb_2 in the Temperature Range of 800°C to 1500°C," *J. Electrochem. Soc.: Solid State Sci.*, **118** [7] 1195–9 (1971).

[20]W. G. Fahrenholtz, "The ZrB_2 Volatility Diagram," *J. Amer. Ceram. Soc.*, **88** [12] 3509–12 (2005).

[21]R. Loehman, E. Corral, H. P. Dumm, P. Kotula, and R. Tandon, "Ultra High Temperature Ceramics for Hypersonic Vehicle Applications"; *Sandia Report* 2006–2925 (2006).

[22]O. Kida and Y. Segawa ZrB_2 Composite Sintered Material, U.S. Patent 4,668,643 (1987).

[23]K. Isozaki, H. Matsunaga, and Y. Imamura, "Sintered Body Having High Corrosion Resistance and Containing ZrB_2"; U.S. Patent 4,952,532, 1990.

[24]S. Levine, E. Opila, M. Halbig, J. Kiser, M. Singh, and J. Salem, "Evaluation of Ultra-High Temperature Ceramics for Aeropropulsion Use," *J. Eur. Ceram. Soc.*, **22**, 2757–67 (2002).

[25]J. She, J.-F. Yang, D. D. Jayaseelan, N. Kondo, T. Ohij, and S. Kanzaki, "Thermal Shock Behavior of Isotropic and Anisotropic Porous Silicon Nitride," *J. Am. Ceram. Soc.*, **86** [4] 738–40 (2003).

[26]D. Munz and T. Fett, "Thermal Shock Behaviour"; pp. 203–26 in *Ceramics—Mechanical Properties, Failure Behaviour, Materials Selection*, Edited by D. Muntz and T Fett. Springer Verlag, Berlin, 1999.

[27]D. P. H. Hasselman, "Thermal Stress Resistance Parameters for Brittle Refractory Ceramics: A Compendium," *Ceram. Bull.*, **49** [12] 1033–7 (1970).

[28]F. de Mestral and F. Thevenot, "Ceramic Composites: TiB_2–TiC–SiC—Part II. Optimization of the Composite 20% TiB_2–55% (mol%) TiC–25% SiC," *J. Mater. Sci.*, **26**, 5561–5 (1991).

[29]C. Aksel and F. Riley, "Young's Modulus Measurements of Magnesia-Spinel Composites Using Load-Deflection Curves, Sonic Modulus, Strain Gauges and Rayleigh Waves," *Journal Title: J. Eur. Ceram. Soc.*, **23**, 3089–96 (2003).

[30]S. Maensiri and S. G. Roberts, "Thermal Shock of Ground and Polished Alumina and Al_2O_3/SiC Nanocomposites," *J. Eur. Ceram. Soc.*, **22**, 2945–56 (2002).

[31]C. Aksel, B. Rand, F. Riley, and P. Warren, "Thermal Shock Behaviour of Magnesia-Spinel Composites," *J. Eur. Ceram. Soc.*, **24**, 2839–45 (2004).

[32]L. Bergero, V. Sglavo, and G. D. Soraru, "Processing and Thermal Shock Resistance of a Polymer-Derived $MoSi_2$/SiCO Ceramic Composite," *J. Am. Ceram. Soc.*, **88** [11] 3222–5 (2005).

[33]P. Becher, D. Lewis III, K. Carman, and A. Gonzalez, "Thermal Shock Resistance of Ceramics: Size and Geometry Effects in Quench Tests," *Ceram. Bull.*, **59** [5] 542–8 (1980).

[34]D. Lewis, "Comparison of Critical dT_C Values in Thermal Shock with the R Parameter," *J. Amer. Ceram. Soc.—Discussions Notes*, **63** [11–12] 713–4 (1980).

[35]L. Scatteia, R. Borrelli, G. Cosentino, E. Bêche, J. L. Sans, and M. Balat-Pichelin, "Catalytic and Radiative Behaviors of ZrB_2–SiC Ultra High Temperature Ceramic Composites," *J. Spacecrafts Rockets*, **43**, 1004–12 (2006).

[36]D. G. Munz, J. L. Shannon Jr, and R. T. Bubsey, "Fracture Toughness Calculation from Maximum Load in Four Point Bend Tests of Chevron Notch Specimens," *Int. J. Fract*, **16**, R137–41 (1980).

[37]F. Monteverde and A. Bellosi, "Development and Characterisation of Metal-Diboride-Base Composites Toughened With Ultra-Fine SiC Particulates," *Solid State Sci*., **7**, 622–30 (2005).
[38]D. Thomas, "Design and Analysis of UHTC Leading Edge Attachment"; NASA/CR–2002-211505 (2002).
[39]A. Chamberlain, W. Fahrenholtz, and G. Hilmas, "Pressureless Sintering of Zirconium Diboride," *J. Am. Ceram. Soc*., **89** [2] 450–6 (2006).
[40]S. Baik and P. Becher, "Effect of Oxygen Contamination on Densification of TiB_2," *J. Am. Ceram. Soc*., **70** [8] 527–30 (1987).
[41]S. Torizuka, K. Sato, H. Nishio, and T. Kishi, "Effect of SiC on Interfacial Reaction and Sintering of TiB_2," *J. Am. Ceram. Soc*., **78** [6] 1606–10 (1995).
[42]F. Monteverde, C. Melandri, and S. Guicciardi, "Microstructure and Mechanical Properties of an HfB_2+ 30vol% SiC Composite Consolidated by Spark Plasma Sintering," *Mat. Chem. Phys*., **100** [2–3] 513–9 (2006).
[43]E. Lutz, M. Swain, and N. Claussen, "Thermal Shock Behavior of Duplex Ceramics," *J. Am. Ceram. Soc*., **74** [1] 19–24 (1991).
[44]Y. Kim and W.-J. Lee, "Case E.D. The Measurement of the Surface Heat Transfer Coefficient for Ceramics Quenched into a Water Bath," *Mater. Sci. Eng*., **A145**, L7–11 (1991).
[45]D. Lewis III, "Thermal Shock and Thermal Shock Fatigue Testing of Ceramics With the Water Quench Test"; pp. 487–96 in *Fracture Mechanics of Ceramics*, Vol. 6. Edited by R. C. Bradt, A. G. Evans, D. P. H. Hasselman, and F. F. Lange. Plenum Press, New York, 1983.
[46]B. Budianski and R. J. O'Connell, "Elastic Moduli of a Cracked Solid," *Int. J. Solids Struc*., **12**, 81–97 (1976).
[47]F. Monteverde, "The Thermal Stability in Air of Hot-Pressed Diboride Matrix Composites for Uses at Ultra-High-Temperatures," *Corr. Sci*., **47**, 2020–33 (2005).
[48]A. Gulbransen and S. A. Jansson, "High-Temperature Oxidation, Reduction and Volatilisation Reaction of Silicon and Silicon Carbide," *Oxid. Methods*, **4**, 181–201 (1972).
[49]W. G. Fahrenholtz, "Thermodynamic Analysis of ZrB_2–SiC Oxidation: Formation of a SiC-Depletd Region," *J. Am. Ceram. Soc*., **90** [1] 143–8 (2007).
[50]A. H. Heuer and V. L. K. Lou, "Volatility Diagrams of Silica, Silicon Nitride and Silicon Carbide," *J. Am. Ceram. Soc*., **73** [10] 2789–803 (1990).
[51]W. Vaughn and H. Maahs, "Active-to-Passive Transition in the Oxidation of Silicon Carbide and Silicon Nitride in Air," *J. Am. Ceram. Soc*., **73** [6] 1540–3 (1990). □